

See discussions, stats, and author profiles for this publication at: <https://www.researchgate.net/publication/325974883>

# Numerical comparison of lattice unit cell designs for medical implants by additive manufacturing

Article in *Virtual and Physical Prototyping* · June 2018

DOI: 10.1080/17452759.2018.1491713

CITATIONS

2

READS

201

5 authors, including:



[Anton Du Plessis](#)

Stellenbosch University

125 PUBLICATIONS 478 CITATIONS

[SEE PROFILE](#)



[Ina Yadroitsava](#)

Central University of Technology

40 PUBLICATIONS 724 CITATIONS

[SEE PROFILE](#)



[Igor Yadroitsev](#)

Central University of Technology

97 PUBLICATIONS 2,253 CITATIONS

[SEE PROFILE](#)



[Deborah Clare Blaine](#)

Stellenbosch University

40 PUBLICATIONS 293 CITATIONS

[SEE PROFILE](#)

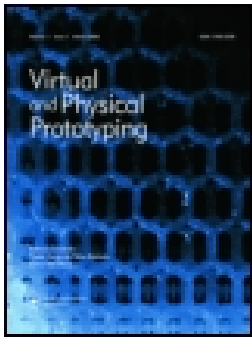
Some of the authors of this publication are also working on these related projects:



Post doc at University of Stellenbosch [View project](#)



Mechanical Properties of High Performance Concrete with Superabsorbent Polymers (SAP) [View project](#)



## Numerical comparison of lattice unit cell designs for medical implants by additive manufacturing

A du Plessis, I Yadroitsava, I Yadroitsev, SG le Roux & DC Blaine

To cite this article: A du Plessis, I Yadroitsava, I Yadroitsev, SG le Roux & DC Blaine (2018): Numerical comparison of lattice unit cell designs for medical implants by additive manufacturing, Virtual and Physical Prototyping, DOI: [10.1080/17452759.2018.1491713](https://doi.org/10.1080/17452759.2018.1491713)

To link to this article: <https://doi.org/10.1080/17452759.2018.1491713>



Published online: 25 Jun 2018.



Submit your article to this journal [↗](#)




View related articles [↗](#)



View Crossmark data [↗](#)



# Numerical comparison of lattice unit cell designs for medical implants by additive manufacturing

A du Plessis <sup>a,b</sup>, I Yadroitsava<sup>c</sup>, I Yadroitsev<sup>c</sup>, SG le Roux<sup>a</sup> and DC Blaine<sup>d</sup>

<sup>a</sup>CT Scanner Facility, University of Stellenbosch, Stellenbosch, South Africa; <sup>b</sup>Physics Department, University of Stellenbosch, Stellenbosch, South Africa; <sup>c</sup>Department of Mechanical and Mechatronic Engineering, Central University of Technology, Bloemfontein, South Africa; <sup>d</sup>Department of Mechanical and Mechatronic Engineering, University of Stellenbosch, Stellenbosch, South Africa

## ABSTRACT

The aim of this study was to compare traditional strut-based lattices with minimal surface designs using morphological analysis and image-based simulations of design files. While the two types have been studied widely, no direct comparison has ever been done. Surprisingly, there are no major differences in performance between the two types generally, but minimal surface designs do outperform slightly on angular load simulation. However, minimal surface designs in this density range are shown to have very thin walls, potentially making their accurate production more challenging, or more suitable for applications where larger pore sizes and sheet thicknesses may be applicable. Interesting results such as dual pore size distributions and variations in tortuosity of pore networks are demonstrated, with differences between various designs. The results show that all the tested designs are suitable for bone implants, but the best design might be selected based on its specialised performance requirements.

## ARTICLE HISTORY

Received 28 May 2018  
Accepted 19 June 2018

## KEYWORDS

Lattice structures; additive manufacturing; bone implants; geometric design

## 1. Introduction

Additive Manufacturing (AM) is a fast-growing class of technologies that uses 3D CAD files to produce complex parts in a layer-by-layer method (Gibson *et al.* 2010; Frazier 2014; Gu *et al.* 2012). In powder bed fusion (PBF), each layer of metal powder is melted using a laser or electron beam, melting only the required areas by scanning the beam across the surface. A new powder layer covers the fused layer and the process continues until the final part is completed and removed from the substrate. One of the advantages of this PBF technology is the ability to produce highly complex parts, allowing many new lightweight designs to be realised easily (Hollister 2005; Orme *et al.* 2017). Such lightweight designs are useful in aerospace and automotive industries, where strength and mass are most important (Lim *et al.* 2016). Another application is in the medical field, where bone replacement implants can effectively use lattice and functionally graded structures. Lattice structures are useful for the osseointegration process, while the stiffness of the structure can be matched to that of the bone, eliminating stress-shielding effects typical of current implants (Zadpoor 2017).

Due to their widespread applications, additively manufactured lattice structures have been the topic of many studies in recent years. As described in Hollister (2005),

the porosity and stiffness of the lattice structure are inter-related. This ratio is well described for foams by the models of Ashby-Gibson (Gibson and Ashby 1999; Ashby *et al.* 2000), and these relations also generally hold well for lattices – the stiffness can be predicted from the porosity of the structure. However, different unit cell designs can alter the mechanical properties, i.e. for the same porosity, the stiffness can be different for different designs. Ahmadi *et al.* (2015) have found that mechanical properties vary depending on the type and size of the unit cell, and varies nonlinearly with porosity. Various unit cell designs have been investigated including for example regular cube-designs (Parthasarathy *et al.* 2010; Sallica-Leva *et al.* 2013), diamond (Ahmadi *et al.* 2014), body-centred cubic and a variation of this with a vertical pillar included (Smith *et al.* 2013) and minimal surface designs (Bobbert *et al.* 2017). One recent study also compared the mechanical properties of different strut-based lattice unit cell types and densities numerically and compared these to experimental data available (Hedayati *et al.* 2018). More generally, a recent review summarised the analytical relationships available to calculate mechanical properties of a range of lattices (Zadpoor and Hedayati 2016). In particular, the analytical and numerical simulated performance of a range of strut-based lattices is reported in Hedayati

*et al.* (2016). The authors showed that the unit cell type and its relative strut length and cross section affect the mechanical properties.

The particular requirements of lattices for bone replacement implants have been described in detail in a number of recent reviews (Wang *et al.* 2016; Tan *et al.* 2017; Murr 2017; Zhang *et al.* 2017; Dong *et al.* 2017). The primary considerations for bone replacement implants are good strength, with the lattice allowing the stiffness of the metallic structure to match that of bone more closely, to minimise stress shielding. The lattice allows in-growth of new bone, thereby attaching itself better in the longer term. This osseointegration occurs by a combination of physiological processes: initial cell seeding, followed by vascularisation and bone growth. Initial cell seeding is strongly dependent on the available surface area for cell attachment, and indications are that lower permeability regions allow for better initial cell seeding, which can be found in irregular cavities and non-spherical pore shapes. For later vascularisation and effective bone growth, good permeability is required to allow nutrients to flow through the structure. These parameters were described in more detail in these reviews, but it is clear that these complex design criteria are not easily matched in one custom design. For this reason, various available designs should be compared for these properties, and more generally the strut-based and minimal surface designs compared to see which are more suitable for bone replacement implants.

Morphological analysis is required since the design is typically specified by unit cell size and density, not by strut thickness or pore size. Therefore, strut thickness and pore size is not a direct input into the design of a periodic lattice structure and it needs to be measured or confirmed once designed. Due to the complexity of the lattice unit cell designs, the measurement of these features is not trivial. A lattice structure morphological analysis is typically made using image processing methods, similar to that done for bone structural analysis. The most widely used method is to measure trabecular thickness and spacing from 2D sections. These can be either directly at individual locations, or using stereological methods – using the circumference and area of the structure of interest in 2D (Thomsen *et al.* 2005). With the availability of microCT imaging, more accurate 3D thickness measurements could be made from 3D images, with two methods widely in use as described in Thomsen *et al.* (2005), Hildebrand and Rüegsegger (1997), Hildebrand *et al.* (1999). One method is to use the same stereological methods, but making use of surface areas and volumes of the features of interest, which are often reported as trabecular thickness TbTh

and trabecular spacing TbSp. However, a more direct and more accurate method is the use of a maximal spheres method. This measures the actual thickness distribution from the 3D structure, as demonstrated for trabecular bone (Hildebrand and Rüegsegger 1997; Hildebrand *et al.* 1999) and is implemented in the software boneJ (Doube *et al.* 2010), for example. However, the method used in various studies is not always well documented (it is not always clear which of the two 3D methods are used).

MicroCT or voxel data can be used for image-based simulations, to better understand the lattice properties. Permeability simulations are performed using a Lattice–Boltzmann method, to simulate Stokes flow (Succi 2001). Static load simulations are carried out using an immersed-boundary finite element code, which allows direct simulation on a voxel data set, without a need for a surface mesh. This method has been applied in recent studies with great success (Fieres *et al.* 2018; du Plessis *et al.* 2017; Broeckhoven *et al.* 2017; Broeckhoven and du Plessis 2017). Mesh-free simulation methods were first shown to be useful in Shapiro and Tsukanov (1999), Freytag *et al.* (2011). The advantage of these methods is the simplicity of using direct simulations on voxel data without the need for meshing. In this work, the additional advantage was that morphological analysis and simulation could be done in the same software package.

The purpose of this work was to compare strut-based and minimal surface designs for their application in bone replacement implants, to identify which type is best for this application. Both of these types have been produced by AM and showed positive results in various investigations (Ahmadi *et al.* 2015; Parthasarathy *et al.* 2010; Sallica-Leva *et al.* 2013; Ahmadi *et al.* 2014; Smith *et al.* 2013; Bobbert *et al.* 2017; Yan *et al.* 2015; Arabnejad *et al.* 2016), but a direct comparison has not yet been reported. We used four strut-based and four minimal surface designs and selected a total porosity of about 60–65% to compare the designs. The advantage of using purely numerical comparisons in this work is to eliminate sources of potential manufacturing or experimental differences, e.g. smaller pore spaces in one design might result in more partially melted material blocking pore spaces, decreasing the experimentally measured permeability for that model. While some of this information could be obtained from analytical models, these are not available for all lattice designs.

For the detailed morphological comparison, we made use of 3D analyses of the pore size distribution, strut size distribution and surface area of each model. As has been mentioned, a larger surface area is preferred for cell seeding, while an ideal porosity percentage, pore size

and shape is a very disputable issue. Wide ranges for micro- and macro pores with sizes of 50–1200  $\mu\text{m}$  were indicated for new bone growth and high fixation in orthopaedic or dental applications (Bobyn *et al.* 1980; Vasconcellos *et al.* 2010; Taniguchi *et al.* 2016; Lopez-Heredia *et al.* 2008), but the optimum pore size for the replacements of human bones still has not been exactly defined (Nouri *et al.* 2009). Despite this, the pore size differences between models are of interest, especially for future osseointegration studies.

For AM lattice structures, struts should be thick enough to enable their accurate production using typical commercial powder bed AM systems. For this purpose, the struts should be as thick as possible, because they have to be at least wider than a single track produced with a certain laser spot size and energy input, from powder that also has limitations since the typical powder bed additive system uses 20–50  $\mu\text{m}$  powder particle sizes. The process parameters defining the track width, i.e. the laser power, scan speed and layer thickness can also affect the build accuracy and quality. This can potentially cause variations in thickness between vertical, diagonal and horizontal struts in lattice structures as demonstrated by Sing *et al.* (2018). It was found that – for the size of lattices investigated – horizontal struts were most sensitive to layer thickness, while vertical and diagonal struts were most sensitive to laser power. It is also possible to compensate for this type of manufacturing error for lattice struts, as demonstrated by Bagheri *et al.* (2017). The authors used a test part to calculate thickness differences at different build angles and use this information as feedback/input to produce more accurate lattices.

In addition to morphological analysis, permeability simulations were performed to directly compare minimal surface and strut-based designs for their laminar flow properties. Higher permeability should result in the better flow of nutrients and hence better bone growth, while the flow complexity (tortuosity) might improve the initial cell seeding and improve the delivery of nutrients to all parts of the lattice. Similarly,

static load simulations were carried out to highlight designs with stress concentrations and predict which models lack such stress concentrations and hence should be stronger, and to identify the predicted elastic modulus of each. In addition to direct loading in parallel to vertical struts, angular load at 45 degrees was simulated on each model to highlight anisotropy in load-induced stresses, i.e. highlighting which designs are better for angular loads.

The study involved detailed 3D morphological analysis of strut/sheet thickness and pore size distributions, and simulations of permeability and static loading stress. In this way, all the important parameters for bone implant applications can be directly compared between the lattice models.


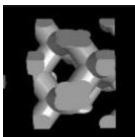
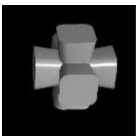

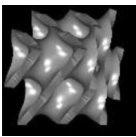
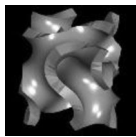
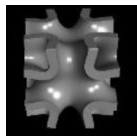
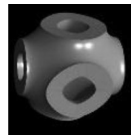
## 2. Materials and methods

The models were selected based on recently published work by Bobbert *et al.* (2017) (minimal surface designs) and typical strut-based models available in commercial AM design software, these are shown in Table 1.

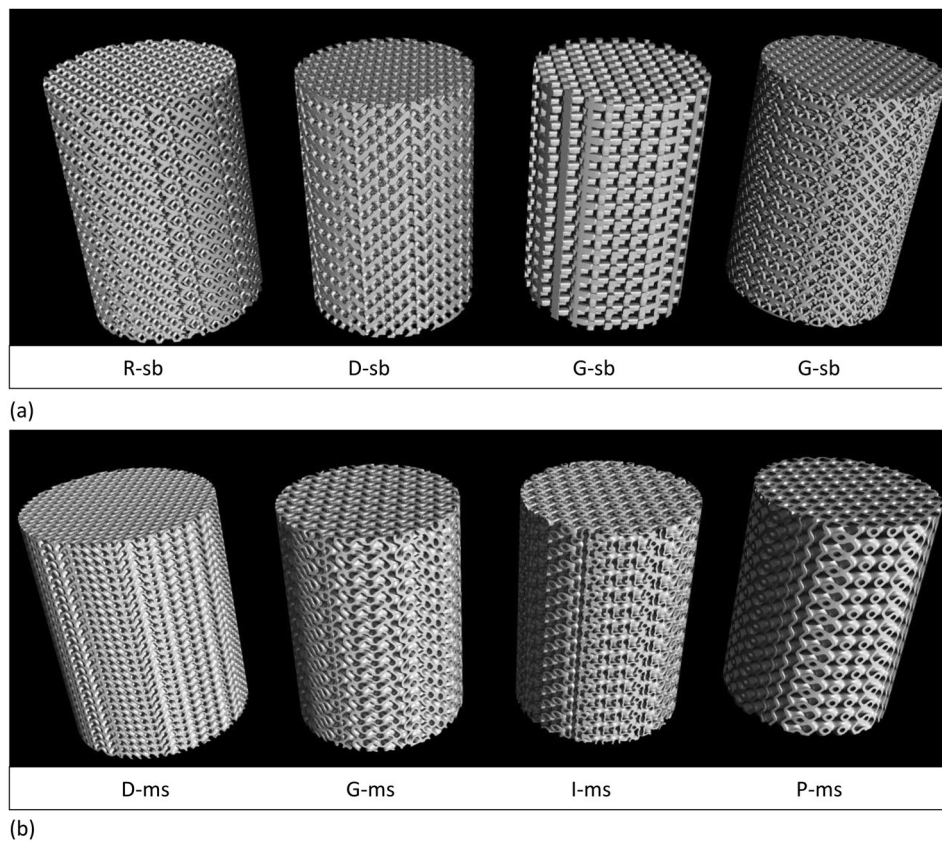
Short names for the models are used for simplicity in this paper, with ‘ms’ referring to minimal surface, and ‘sb’ referring to strut-based designs. For strut-based designs, the selected designs were used: Rhombic dodecahedron (R-sb), Diamond (D-sb), G-struct (G-sb) and Octet (O-sb). The unit cells for these were obtained in Materialize Magics, and tessellated cylinders generated using a 1.5 mm unit cell size, with total 15 mm width of cylinder and 22.5 mm height, Figure 1(a). The same criteria were applied to minimal surface designs, but models were obtained as used in a previous study by Bobbert *et al.* (2017). These sample sizes correspond to suggested sample sizes for compression tests of porous metal samples according to ISO 13314-2011.

The minimal surface designs investigated where the Diamond (D-ms), Gyroid (G-ms), Isometric Wrapped Surface – also known as I-WP (I-ms) and Primitive (P-ms), Figure 1(b). Four different porosities of each

**Table 1.** Investigated designs for lattice structures.

	Strut-based design				Minimal surface design			
	Rhombic dodecahedron	Diamond	G-struct	Octet	Diamond	Gyroid	I-WP	Primitive
								
		D-sb	G-sb	O-sb	D-ms	G-ms	I-ms	P-ms
Porosity, %								
63		61	63	62	62	63	65	62
Strut/Sheet thickness, $\mu\text{m}$								
332		491	651	288	157	188	152	250





**Figure 1.** Different designs selected for comparison of (a) strut-based lattices and (b) minimal surfaces.

model were created. Basic morphological assessment of material fraction, allowed a selection of one of each type corresponding to 35–39% material fraction (65–61% porosity total), for further investigations. The models with similar total porosity shown in Figure 1 have varying strut or sheet thicknesses. Generally, the minimal surface designs have thinner sheets than the strut thickness in strut-based designs (see Table 1), for similar total density.

All analyses were performed in Volume Graphics VGstudiomax 3.1. The STL data were converted to voxel data using the function ‘convert to volume’, resulting in effective voxel sizes of approximately  $12\ \mu\text{m}$ , with a total volume size of approximately  $1300 \times 1300 \times 1900$  voxels.

The basic morphological analysis – i.e. the measurement of strut thickness and pore size – is necessary because the models are typically created with a choice of unit cell size and density. This does not provide a clear choice of pore size or strut thickness to a design engineer. Different designs might produce different strut thicknesses and pore sizes for the same average density. In this work, three methods were employed to accurately compare models.

The simplest method is to measure the strut thickness and pore size using 2D sectioning and image

analysis. The second morphological analysis method involves a 3D stereological method, which is a fast method widely in use: calculations based on the total volume and surface area of the structure. These typical morphological parameters include total surface area, material or bone volume to total volume (BV/TV), trabecular thickness (TbTh), and trabecular spacing (TbSp). These are calculated from volume and surface area of the structure according to the stereological methods described in (Thomsen *et al.* 2005; Hildebrand and Rüegsegger 1997; Hildebrand *et al.* 1999) and this method is widely in use in biomedical bone analysis, hence the terminology. The third morphological analysis method is expected to be the most accurate since it uses a more advanced direct 3D measurement using a maximal spheres method – e.g. for strut thickness analysis, the diameter of the largest sphere that fits in a given region in the strut is reported as the strut diameter at that location, and this is repeated across all points within the structure resulting in a statistical analysis result providing a thickness value at every point in the structure. This method has been described previously (Hildebrand and Rüegsegger 1997; Hildebrand *et al.* 1999) and is also implemented in other software such as boneJ (Doubé *et al.* 2010). This method is used for quantification of

3D structures such as bone (Thomsen *et al.* 2005; Hildebrand and Rüegsegger 1997; Hildebrand *et al.* 1999; Doube *et al.* 2010), but the use of this method or the stereological 3D method is not always well described or differentiated in the literature, and this direct measurement is more computationally intensive.

The maximal sphere method was applied to measure the detailed strut thickness and pore size distributions for all models. For these analyses, the data were cropped on the edges of the cylinder to ensure no edge errors from surrounding air in the model. The strut and pore size distributions are shown to be non-normal, therefore we propose median thickness as a better method to describe lattice structures. Previous work, especially in bone analysis, has generally reported mean values (Hildebrand and Rüegsegger 1997; Hildebrand *et al.* 1999; Doube *et al.* 2010).

For absolute permeability simulations (assuming laminar flow in a flooded medium), a Stokes flow simulation was used, which is implemented in the 'transport phenomena' module of VGStudioMax. Default simulation parameters were used including for the dynamic viscosity of water as 0.001 Pa s, inlet and outlet planes at top and bottom of cylinder, and sealed edges ensuring the flow is simulated in the vertical direction along the lattice structure. An arbitrary choice of 1 Pa pressure difference between top and bottom planes was selected to simulate laminar flow. The results provide absolute permeability values as well as tortuosity of the pore network. The tortuosity is defined as the ratio of the

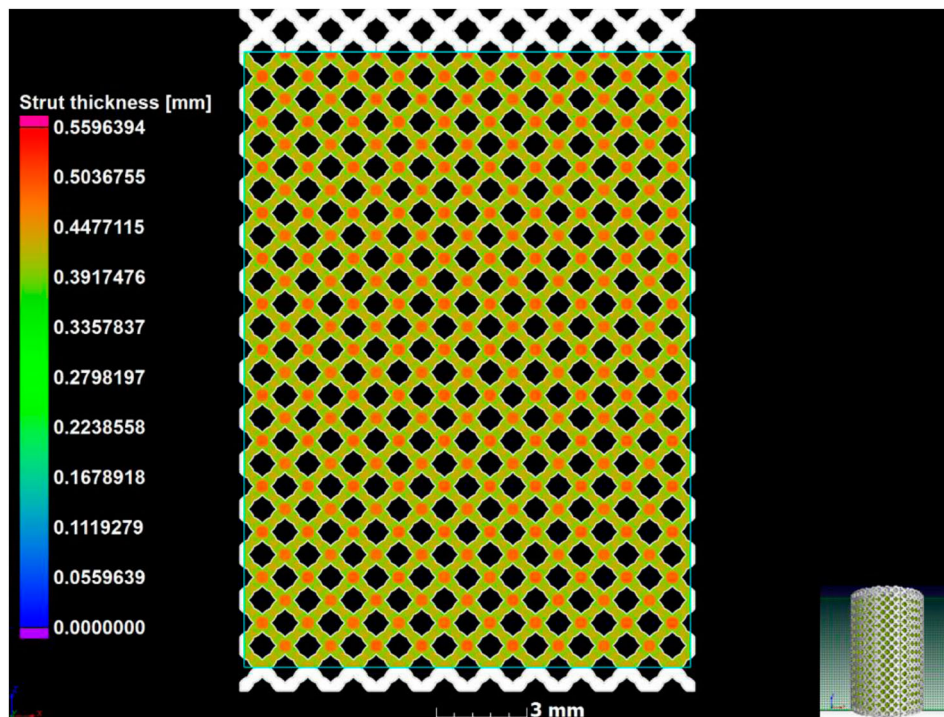
mean flow path length relative to the shortest distance between the flow path inlet and outlet planes.

For static load simulations, an immersed-boundary finite element code was used, which is implemented in the 'structural mechanics' module of VGStudioMax, with an arbitrary choice of 1 kN load applied, assuming linear elastic isotropic material parameters, with 115 GPa for the Young's modulus of Ti6Al4V and Poisson's ratio 0.3. The base of the cylinder was fixed in all degrees of freedom in a region covering the bottom 0.15 mm of the cylinder while the same size area along the top of the lattice was used as the load application area. The same procedure as in previous studies (du Plessis *et al.* 2017; Broeckhoven *et al.* 2017; Broeckhoven and du Plessis 2017) was applied here, with simulation cell size of 40  $\mu\text{m}$  for all lattices. In this work, distributed computing was required to allow the large data sets to be simulated at this small unit size, using two large workstations in parallel. Results obtained were recorded as the mean of the maximum 1% interval of Von Mises stresses, as applied previously. Finally, static load simulations were also applied with loading at a 45-degree angle relative to the vertical.

### 3. Results and discussion

#### 3.1 Morphological analysis

For design files, basic morphological analysis of strut thickness and pore size is required since these are not



**Figure 2.** Measurement of strut thickness using maximal spheres method for the Rhombic dodecahedron strut-based sample (R-sb).

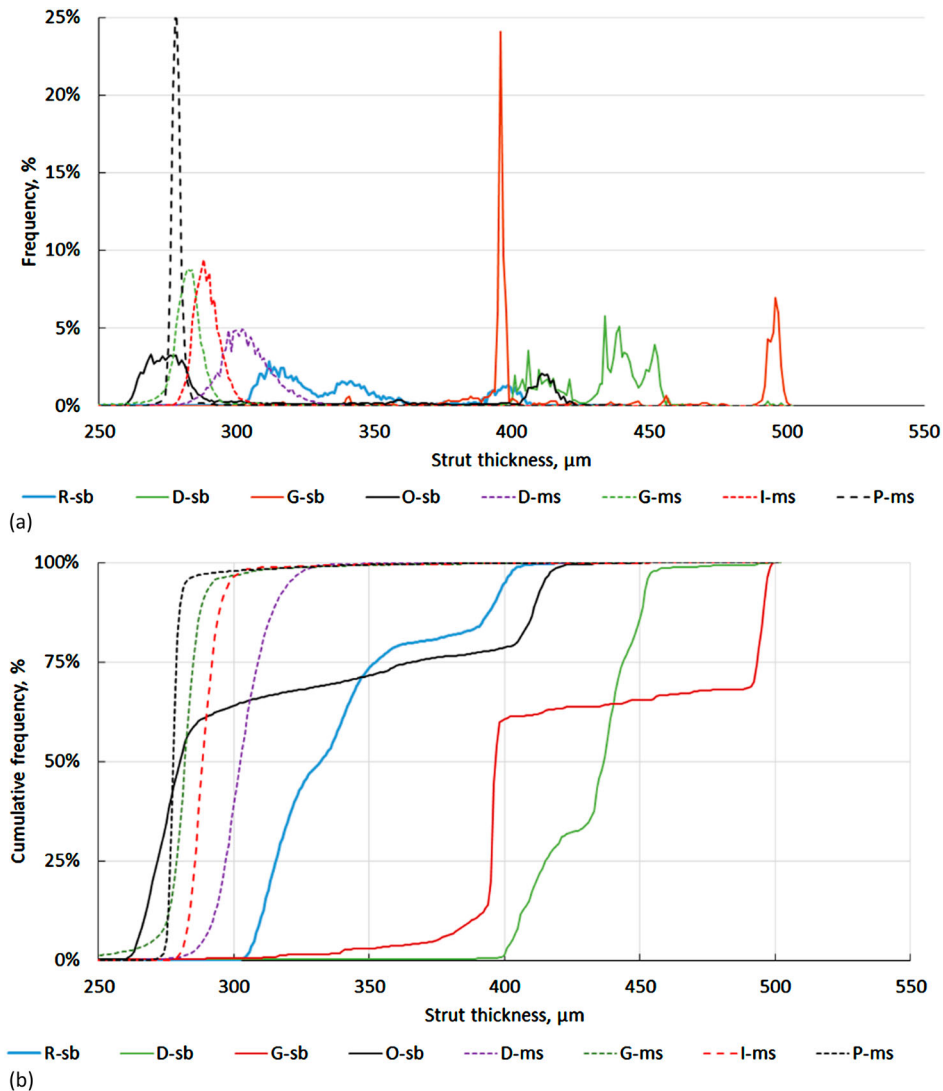
inputs in the design phase, and can vary depending on the type of the unit cell selected or the size of the unit cell selected.

### 3.1.1 Strut thickness

A typical result for a maximal spheres thickness analysis of the strut thickness is shown in Figure 2. Clearly, the junctions are thicker than the struts alone. This is an example of a Rhombic dodecahedron design, but this method was applied to all 8 models of similar porosity and the strut thickness distributions graphed as shown in Figure 3.

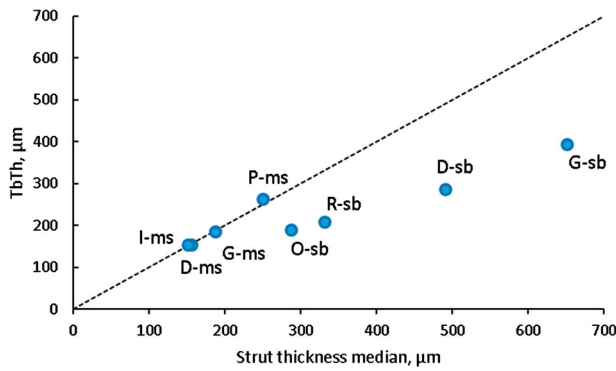
Clearly, the strut thickness distributions are non-trivial and vary considerably between designs. In particular, it seems the minimal surface designs have a single 'thickness' value, which makes sense as they are designed as sheets. The strut-based designs contain variations of thicknesses due to their different junctions and struts

between them with different dimensions, mostly with a dual-peak distribution (Figure 3(a)). Also observed in Figure 3 are that, for the same porosity, the minimal surface designs have a much lower strut/sheet thickness. This small value is concerning in terms of manufacturability using powder bed AM systems which usually are limited by the track widths under selected process parameters. One way of increasing the thickness of minimal surfaces while keeping the total porosity constant is increasing the unit cell size. This has the disadvantage of increasing the pore size, which might make the structure unsuitable for bone implants. Besides the challenge of manufacturing thin structures, previous work successfully produced such models with good mechanical properties, likely due to the nature of the minimal surface being 'self-supporting' and without sharp corners (Bobbert *et al.* 2017; Yan *et al.* 2015). Therefore, with optimal process parameters, these models can



**Figure 3.** Comparison of 3D strut thickness distribution based on the maximal spheres method for minimal surface and strut-based designs: relative frequencies (a) and cumulative curves (b).





**Figure 4.** Correlation between medians of strut thickness analysis using maximal spheres method and traditional TbTh measurement.

successfully be produced despite the thin strut/sheet thickness.

The maximal spheres method (direct 3D method) was compared to the traditional TbTh measurement (3D stereology) for the same 8 structures across the different models and results are shown in Figure 4. The correlation is good at small thickness values, but the thickness measured using maximal spheres is larger by a factor of 1.7–1.8 compared to the TbTh measurement for large values. This indicates a need to accurately quantify thickness distributions for these type of structures (using maximal spheres method) rather than only make use of stereological measures. This will be especially true when analysing microCT data of real samples, as the surface roughness will increase the

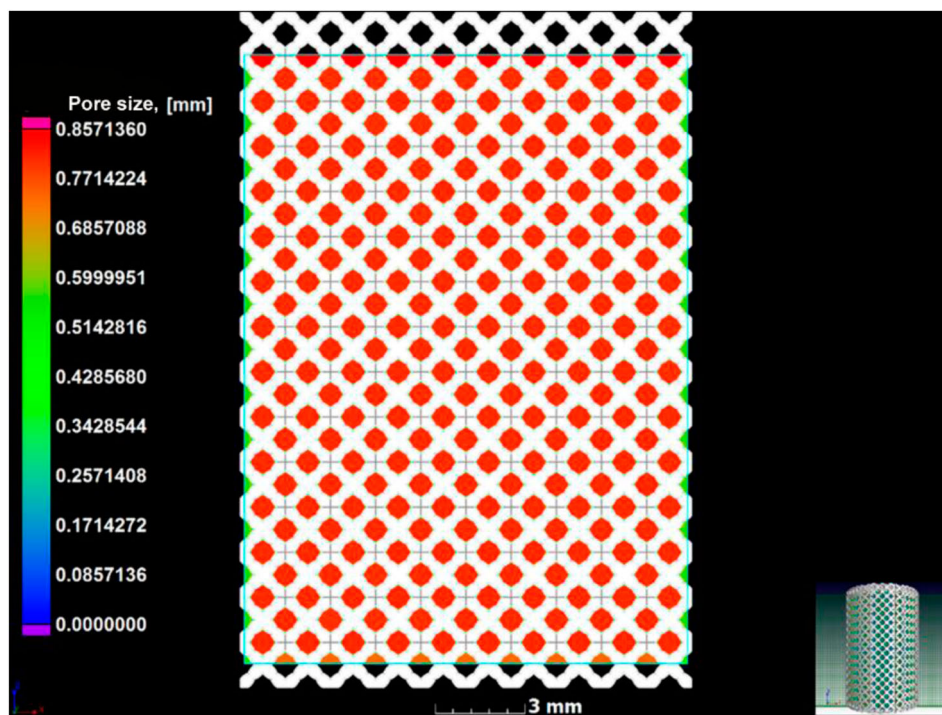
measured total surface area while keeping the total volume constant, further complicating the stereological measurement method.

### 3.1.2 Pore size

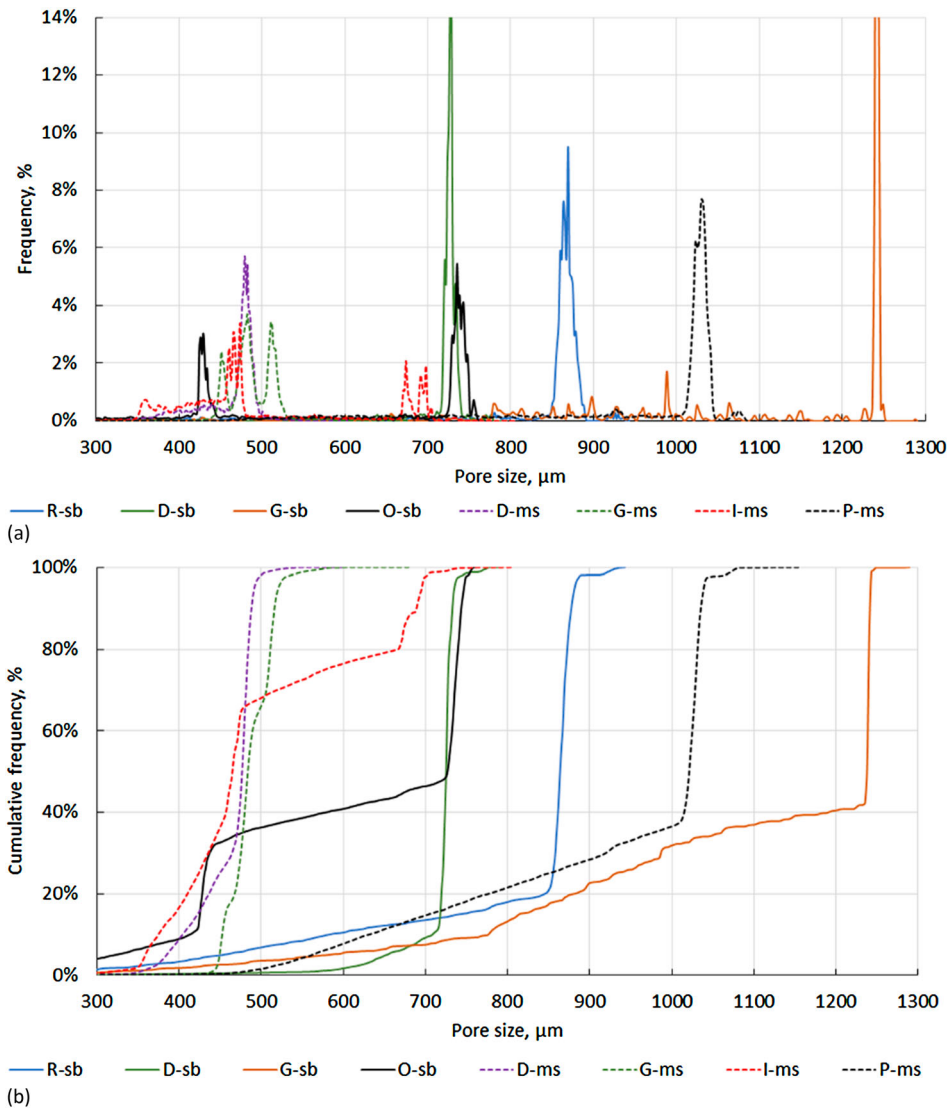
Accurate measurement of pore size is important for lattice designs for bone replacement implants, as the pore size and shape affects the bone growth into the lattice. The maximal spheres measurement of pore size distribution is shown for the Rhombic dodecahedron design in Figure 5.

The resulting pore size distributions for each of the different models are shown in Figure 6. The minimal surface designs show strong variation between models with varying pore sizes. What is surprising is the much larger pore size of the P-ms model compared to other minimal surface designs. For strut-based designs, the pore sizes cover the same range as the minimal surface designs but with more clear peaks, i.e. they are more well defined. In this case, the Octet design is particularly interesting as it shows a clear dual pore size. We assume that such dual pore sizes might be beneficial for cell seeding (requiring smaller pores) and vascularisation and bone growth (requiring larger pores).

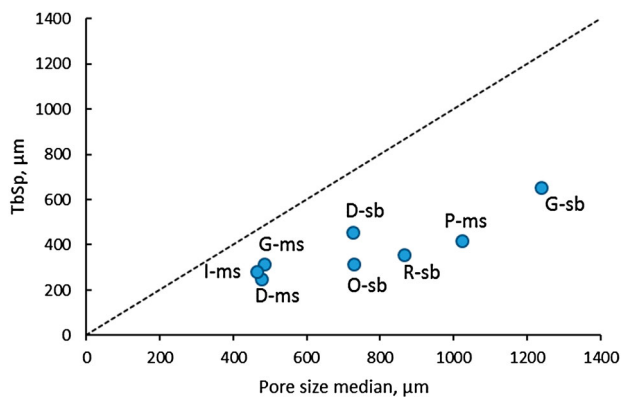
Similar to the procedure in the previous section, the maximal spheres pore size was compared to that obtained by traditional TbSp measurement (3D stereology), as shown in Figure 7. In this case, as before, the pore size is, in reality, larger than the TbSp measurement.



**Figure 5.** Measurement of pore size distribution using maximal spheres method.



**Figure 6.** Comparison of 3D pore size distribution based on the maximal spheres method for minimal surface and strut-based designs: relative frequencies (a) and cumulative curves (b).

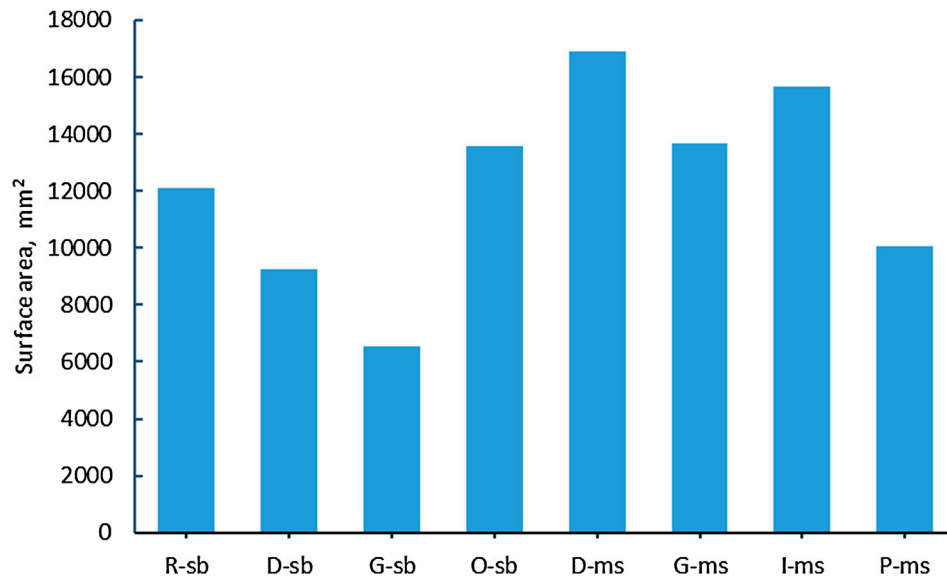


**Figure 7.** Correlation between pore size analysis using maximal spheres method and traditional TbSp measurements.

Once again, this indicates a need to accurately quantify pore sizes in 3D rather than rely on simplified measurements.

### 3.1.3 Surface area

The total surface area of the lattice for bone implants is important since cell seeding takes place on the surface and a larger surface area is thus conducive to improved cell seeding, providing more area for attachment of cells allowing faster and improved initial stages of bone growth. For a direct comparison among the 8 designs, which have the same porosity and total size, the absolute surface area of each is shown in Figure 8. From this, one can see that the minimal surface designs generally have a higher surface area, but not significantly so. One exception is the P-ms



**Figure 8.** Comparison of surface area for different lattice designs of cylinders with 15 mm diameter and 20 mm height, 61–65% porosity.

model which has a lower surface area than the other minimal surface designs. The Octet design O-sb has a relatively high surface area. The lowest surface area design is that of the G-sb lattice, most likely due to its cubic simplified design.

### 3.2 Simulations

#### 3.2.1 Permeability

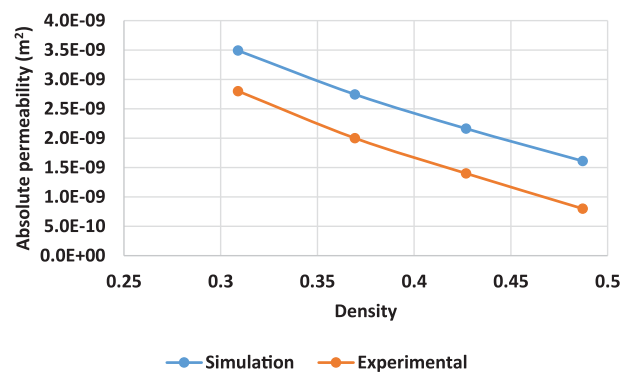
The Lattices must have a high permeability to allow nutrient flow and bone growth, and permeability simulations can be used to predict which designs are suitable for such applications. Such a simulation also provides a tortuosity value, with high values indicating a more complex flow. A higher tortuosity (more complex flow) is presumably required for bone implants to allow some areas to have low flow rates, assisting cell seeding, while other areas have high flow rates allowing the flow of nutrients efficiently.

The permeability simulations were done using a Stokes flow method based on a flooded medium, sealed on the edges, with a pressure difference between inlet and outlet planes. This algorithm is implemented in the voxel-based software package and is based on a simple laminar flow simulation. The absolute permeability and tortuosity were calculated and permeability could be compared directly to experimental data of Bobbert *et al.* (2017) – this was done for the minimal surface design ‘gyroid’ for a range of different densities. These results are shown in Figure 9 – they compare well, with experimental data slightly lower in absolute permeability values. This can be expected since the manufacturing

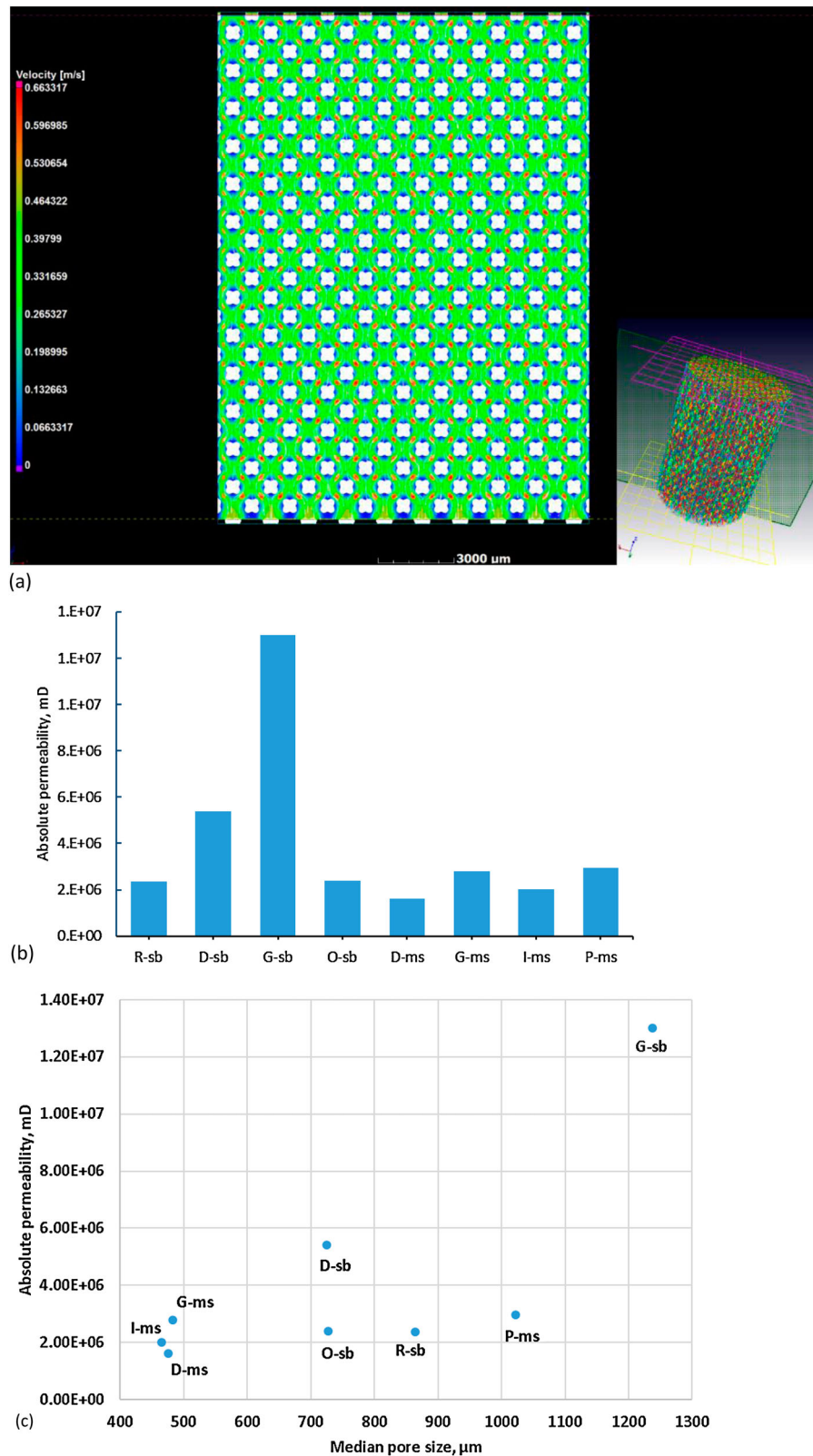
process might result in some parts of the lattices partially blocked by the melted material or partially melted materials that cannot easily be removed.

A typical laminar flow simulation is shown in Figure 10(a) and absolute permeability values calculated from simulations comparing designs in Figure 10(b). A correlation between pore size and permeability is shown in Figure 10(c) indicating a complex relationship depending on lattice design.

The results show that the lowest permeability is found for the D-ms model, making it possibly less suitable for bone implants. The highest permeability is found for the G-sb design, which also has the largest pore size, which is expected. However, the permeability does not scale linearly with pore size as shown in Figure 10(c) and the results do not indicate that



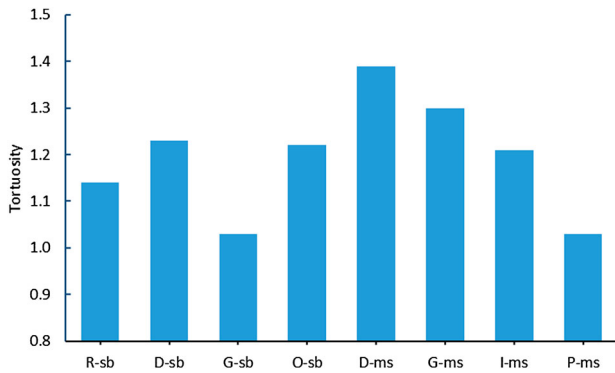
**Figure 9.** Absolute permeability results for gyroid lattices of varying density – simulation in this study vs experimental results from (Bobbert *et al.* 2017).



**Figure 10.** Permeability simulations (laminar flow) showing (a) a slice image of the analysis for the Rhombic dodecahedron lattice, (b) absolute permeability differences between designs, and (c) permeability as a function of median pore size showing a complex relationship.

either the minimal surface or strut-based designs are more or less suitable for permeability applications. What is interesting is that the permeability can vary

significantly for the same pore size and total porosity (e.g. D-sb and O-sb have the same pore size and porosity but significantly different permeability).



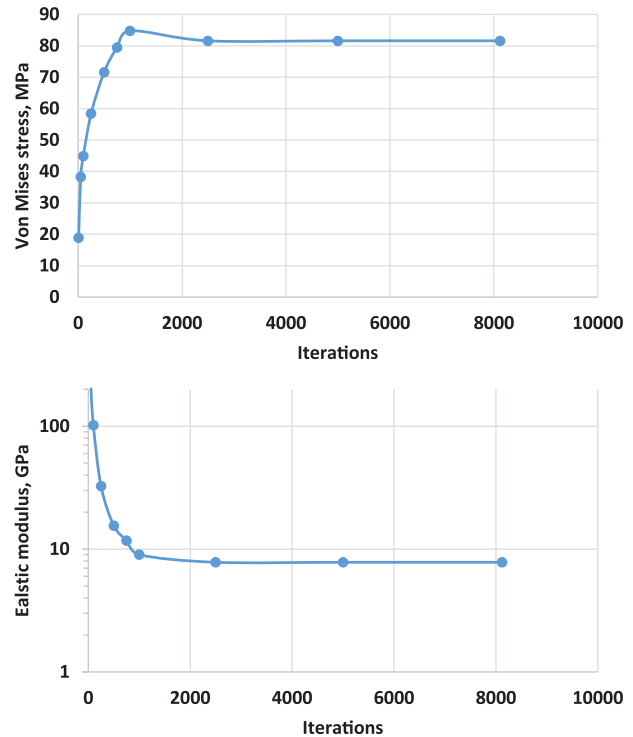
**Figure 11.** Tortuosity of pore network, from permeability simulation.

The rough dependence of permeability on pore size is expected but does not take into consideration the requirement for complex flow of nutrients in medical implants. The flow path complexity can be obtained by the same simulation and is best described by a parameter termed tortuosity, which is a measure of the path length of a typical fluid flow streamline through the medium, compared to a straight line through the same medium. Higher tortuosity can therefore be expected to allow nutrients to reach more areas within the lattice, improving its performance for cell seeding, vascularisation and bone growth. The permeability simulations allow a simple measure of tortuosity, as shown in Figure 11. These results indicate that G-sb has the lowest tortuosity (the structure acts like open channels from top to bottom, but with no flow between them). The P-ms model also has low tortuosity, most likely not making it suitable for bone replacement implants. The other minimal surfaces have good tortuosity, while strut-based models diamond and octet seem reasonable.

### 3.2.2 Static load simulation

The most crucial parameter for lattices to be used in bone replacement implants is the strength and effective elastic modulus. Static load simulations using elastic, homogenous material parameters were used here to directly compare Young's modulus and stress distributions in different lattice designs.

In order to provide confidence in the validity of the structural mechanics simulation method employed in this work, the following approach was followed. In a first series of simulations, the convergence of results was demonstrated: maximum Von Mises stress and effective elastic modulus were recorded with increasing numbers of iterations. Then, simulations for one model of each type was compared to that predicted by the Ashby–Gibson model for open-cell foams. Following this, the model in this work which is most similar to



**Figure 12.** Convergence of 1% maxima for Von Mises stress (top) and Elastic modulus (bottom).

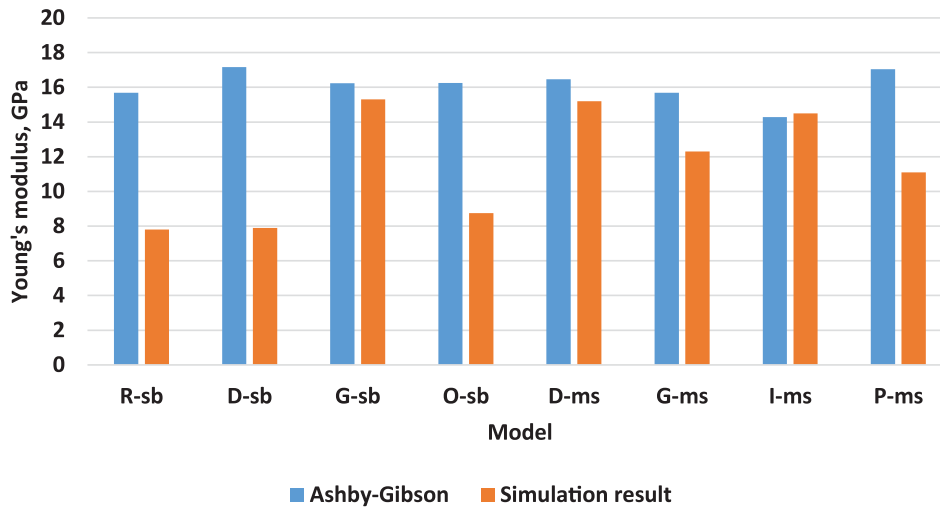
the simple cube-lattice, the G-struct (G-sb), was selected over a range of densities. This was used to compare simulation results with analytical results of both Ashby–Gibson and a beam-based Euler Bernoulli solution. Finally, these results were discussed in relation to similar models for which experimental data is available from the literature.

The Rhombic model (the first one in Figure 1, strut-based design) was employed for convergence tests measuring Von Mises stress maximum and elastic modulus – both are shown in Figure 12. Clearly, the results converge well, providing some confidence in the method, provided more than approx. 2000 iterations were used.

Simulations for each of the 8 models in this work were compared to calculations based on the Ashby–Gibson model for open-cell foams (Gibson and Ashby 1999; Ashby *et al.* 2000). In this comparison, shown in Figure 13, some of the simulation results compare well while some models show lower simulation results for the elastic modulus. This can be expected as the Ashby–Gibson model is a simplified model based on linear square struts in a cube-lattice geometry.

The results in Figure 13 show some complexity, which is one of the reasons simulations should be used to directly compare different designs – the Ashby–Gibson model is only a simplified model based on straight struts, and analytical solutions are not always available





**Figure 13.** Simulation results for elastic modulus compared to prediction from Ashby–Gibson model.

for all models, especially complex mixtures of models or graded structures. One simple model for which an analytical solution is available, is the cube-geometry – this is also the basis of the Ashby–Gibson model. The analytical solution for the cube geometry is taken from (Sing *et al.* 2018; Bagheri *et al.* 2017).

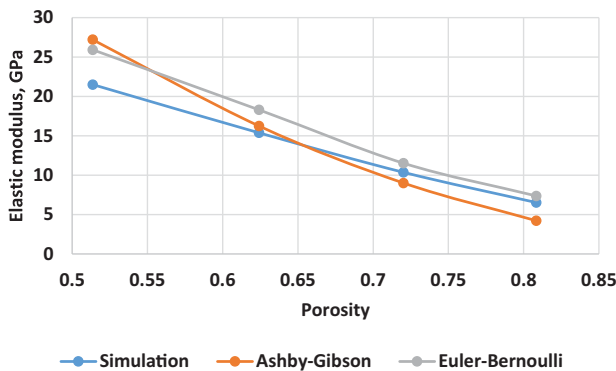
The model used in this study which is the most similar to a cube-lattice is the G-sb (Gstruct model – see Figure 1, third model). For this model, the simulation result shown in Figure 13 is very close to the calculated elastic modulus from the Ashby–Gibson method. For this model, four different densities were selected for further simulations and compared to both analytical models mentioned above. This is shown in Figure 14 and provides further confidence in the simulation results.

When the simulation results for minimal surface designs as in Figure 13 are compared to experimental data of Bobbert *et al.* (2017), the elastic modulus found in their experiments is lower (approx. 5 GPa) compared to both the Ashby–Gibson model and the simulations of this work (11–16 GPa). In a previous study of truncated

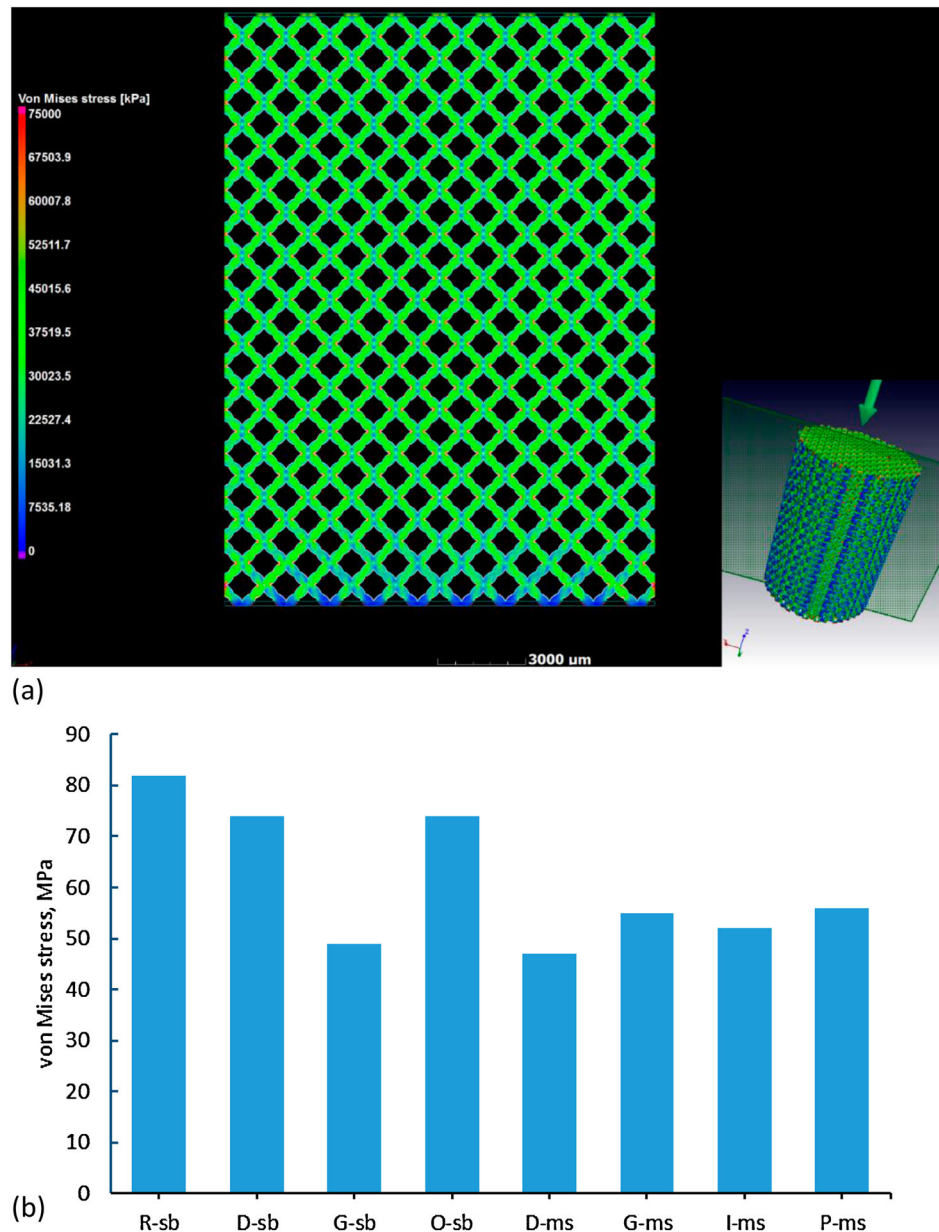
cube lattices (Hedayati *et al.* 2016), a similar effect was observed regarding lower experimental mechanical properties than that predicted by modelling. This effect might be due to various manufacturing imperfections in the PBF process, such as surface roughness, internal defects, microstructure variations or residual stresses, all of which will reduce the strength and elastic modulus, and might vary between models and with different build angles. For example in Sing *et al.* (2016), struts which should have been approximately 0.8 mm where in fact produced in varying thickness depending on production conditions down to as little as 0.2 mm, with significant amounts of partially melted powder on the surface. Such manufacturing influences are eliminated when considering comparisons of designs based only on simulation.

The elastic modulus values obtained in this study for all models were in the range of 8–16 GPa (Figure 13), close to that of cortical or trabecular bone, and all are therefore suitable for bone replacements because stress shielding caused by high stiffness gradients between bones and implants will be avoided.

Lattices with higher stress values and stress concentrations, are likely to have lower static loading yield strength, lower fatigue life and are likely to fail at the location of high stress found in simulation. A typical stress simulation result is shown in Figure 15(a) for the Rhombic dodecahedron strut-based design, while the maximum stress values are compared in Figure 15(b) across the different designs. It is found here that the minimal surfaces all have low-stress values, most likely due to the better distribution of load across the sheet-like structure, while struts have junctions where stress concentrations can be found in corners. One exception is the G-sb model, which has low stress – this can be explained by its vertical struts which are relatively thick.



**Figure 14.** Simulation result vs analytical models for Gstruct model (G-sb) over a range of densities.



**Figure 15.** Static load simulation of 1 kN vertically applied load, showing (a) typical visual von Mises stress distribution in the R-sb lattice and (b) comparison of maximum Von Mises stress for all 8 designs.

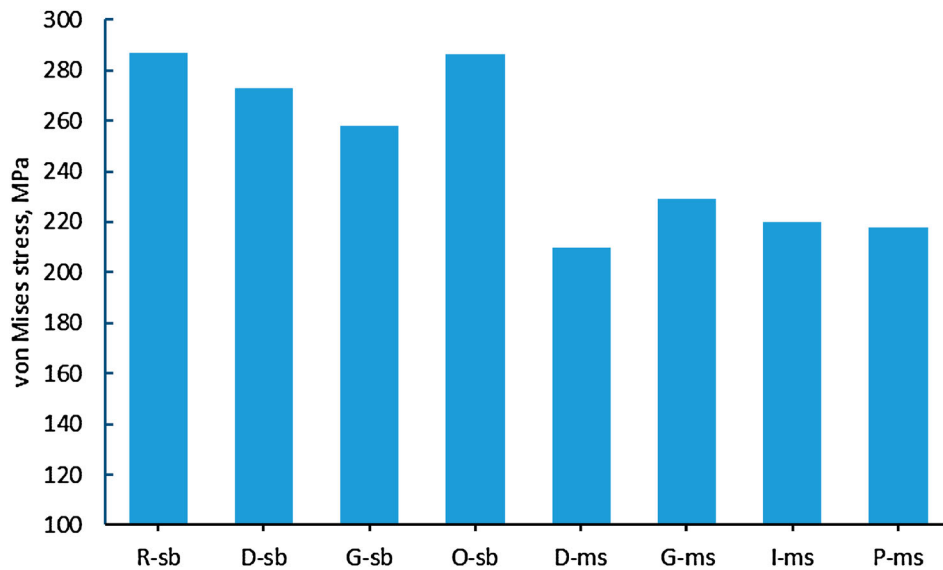
Since the strut-based designs, in particular, are expected to be anisotropic with regards to their mechanical properties, due to the directionality of the struts, load simulations were also done at a 45-degree angle relative to the vertical. These results are shown in Figure 16, clearly show the lower stress in all minimal surface designs compared to higher stress in strut-based designs.

#### 4. Conclusions

This investigation compared minimal surface and strut-based designs for lattice structures directly for the first time, aiming to find the best designs for bone

replacement implants. This was done using a combination of advanced 3D morphological measurements and simulations of permeability and static loading. The strut-based models investigated were Rhombic dodecahedron (R-sb), Diamond (D-sb), Gstruct (G-sb) and Octet (O-sb). The minimal surface designs investigated were Diamond (D-ms), Gyroid (G-ms), I-WP (I-ms) and Primitive (P-ms).

The most important result is that there are no major differences for any of the investigated characteristics between strut-based and minimal surface designs, for the typical implant density. This means that both types of lattices will be suitable generally for this application.



**Figure 16.** Comparison of maximum Von Mises stress for different designs from static load simulations at 45 degrees to vertical.

The only small differences found between the two types are that the minimal surfaces outperform strut-based designs on angular loads. However, they are also shown to have thin sheet thickness compared to the strut thickness for the same density models. This might impact their manufacturability on some PBF systems. Nevertheless, when process parameters are optimised this should not be a limitation, as has been shown before in other studies (Bobbert *et al.* 2017; Yan *et al.* 2015; Clymer *et al.* 2017).

Besides these general results, and despite the minor differences between all models, the following points summarises the comparison and highlights individual properties:

- (1) Strut thickness and pore size distributions show complex non-normal distributions, which might be important for bone implant success, e.g. dual or triple-peaked pore size distributions might be an advantage for bone growth as the small pores allow cell seeding and initial bone growth while larger pores allow vascularisation and later bone ingrowth. All models vary in their pore size distribution profiles. Minimal surface designs are found to have mostly one size for their strut/sheet thickness. Future osseointegration studies could attempt to find not only ideal pore sizes but potentially correlate osseointegration success with complex pore distributions.
- (2) Relative surface areas vary between all designs, with three out of four minimal surfaces having higher than average surface areas but the P-ms having a lower surface area. The D-sb and G-sb also have relatively low surface areas. Surface area is expected to be important for initial cell seeding.
- (3) Permeability varies in all designs, with larger pore sizes resulting in higher permeability, but a non-linear relationship is present: some designs, which have the same pore size median, have different permeability values. Good models for permeability are G-ms, D-sb and G-sb. Tortuosity describes the flow path complexity, with higher flow path complexity assumed to be advantageous for implants, for this it seems the best of the above three models is the G-ms and D-sb models, as the G-sb has the lowest tortuosity
- (4) Load simulations show that the elastic modulus of all models is good and within the range of 8–16 GPa, with minimal surfaces in general slightly higher (stiffer) than strut-based designs.
- (5) Minimal surface designs have low stresses in static load simulation, indicating they distribute the load better and should, therefore, have higher static yield strength. The lack of stress concentration regions (e.g. sharp edges, corners) should increase their fatigue life as well. All minimal surface designs handle angular loads better than strut-based designs.
- (6) Considering all parameters besides strut thickness, the best design seems to be Gyroid and I-WP structures of the minimal surface types, since they have the best combination of good pore size, high surface area, high permeability and high tortuosity of pore network, coupled with low stress under applied load.
- (7) Considering the static load simulation will emphasise sharp corners, which may be smoothed out in real built parts, or even in the design phase, the Octet design also has a reasonably good combination of parameters.

The complexity and inter-relation between parameters make this kind of detailed comparison necessary to ensure best designs are selected for a particular purpose, as in this case for bone replacement implants. When one aspect is considered more important, a suitable model may be selected for this purpose.

It is envisaged that new lattice designs will be tested according to the methodology reported here. An interesting result is the non-trivial pore size and strut thickness distributions, as well as the total surface areas, varying significantly between designs. It would be interesting to correlate future osseointegration studies of bone growth in different lattice designs, with the detailed pore size distributions, permeability, tortuosity and total surface area values found in these simulations.

## Acknowledgements

Johannes Fieres is acknowledged for assisting in setting up the distributed computing capability to allow the structural mechanics simulations on these large data sets. Models for minimal surface designs were obtained from Karel Lietart (3D Systems) and Mohammad Ahmadi (Biomechanical Department of the TU Delft) and they are acknowledged for sharing these files. We also acknowledge Materialise for providing a temporary license of the Magics software to produce models for strut-based designs.

## Disclosure statement

No potential conflict of interest was reported by the authors.

## Funding

This work is based on research supported by the South African Research Chairs Initiative of the Department of Science and Technology and National Research Foundation of South Africa (Grant No. 97994) and the Collaborative Program in Additive Manufacturing (Contract No. CSIR-NLCCPAM-15-MOA-CUT-01).

## Notes on contributors

**Prof. A du Plessis** is Associate Professor at Stellenbosch University. His research interests lie in applications of X-ray microCT, additive manufacturing and biological structures (specifically biomimicry). He has published 80 journal papers.

**Dr. I Yadroitsava** is currently Senior Researcher at Faculty of Engineering and Information Technology, Central University of Technology, Free State. Since 2010, her specific focus and area of research interest are in Additive Manufacturing. She is co-author of more than 40 papers in this field.

**Prof. I Yadroitsev** is Research Professor at Faculty of Engineering and Information Technology, Central University of Technology, Free State. In 2015, he was appointed as SARChI Research Chair in Medical Product Development through Additive Manufacturing. Prof. Yadroitsev has over 30 years of academic experience in Applied Optics & Laser technologies (additive

manufacturing, laser processing, material science, and optics). He has strong interdisciplinary background and extensive experience in the field of Physics and Engineering. He published more than 140 papers and he is a holder of 11 patents.

**Mr. SG le Roux** is Researcher at the Stellenbosch University CT facility. His main expertise is image analysis of X-ray microCT scans. He has published 30 journal papers.

**Prof. DC Blaine** is Associate Professor in Mechanical Engineering, with research interest primarily in Materials Engineering, with a specific focus on powder metallurgy (PM) and the mechanical behaviour of materials. Her current research projects focus on process modelling for PM manufacturing as well as the development and characterisation of PM materials. She has supervised several postgraduate students, published 50 papers and regularly presents her research at international conferences.

## ORCID

A du Plessis  <http://orcid.org/0000-0002-4370-8661>

## References

- Ahmadi, S.M., et al., 2014. Mechanical behavior of regular open-cell porous biomaterials made of diamond lattice unit cells. *Journal of the Mechanical Behavior of Biomedical Materials*, 34, 106–115.
- Ahmadi, S.M., et al., 2015. Additively manufactured open-cell porous biomaterials made from six different space-filling unit cells: The mechanical and morphological properties. *Materials*, 8 (4), 1871–1896.
- Arabnejad, S., et al., 2016. High-strength porous biomaterials for bone replacement: A strategy to assess the interplay between cell morphology, mechanical properties, bone ingrowth and manufacturing constraints. *Acta Biomaterialia*, 30, 345–356.
- Ashby, M.F., et al., 2000. *Metal foams: a design guide*. Boston: Butterworth-Heinemann.
- Bagheri, Z.S., et al., 2017. Compensation strategy to reduce geometry and mechanics mismatches in porous biomaterials built with selective laser melting. *Journal of the Mechanical Behavior of Biomedical Materials*, 70, 17–27.
- Bobbert, F.S.L., et al., 2017. Additively manufactured metallic porous biomaterials based on minimal surfaces: A unique combination of topological, mechanical, and mass transport properties. *Acta Biomaterialia*, 53, 572–584.
- Bobyn, J.D., et al., 1980. The optimum pore size for the fixation of porous-surfaced metal implants by the ingrowth of bone. *Clinical Orthopaedics and Related Research*, 150, 263–270.
- Broeckhoven, C., and du Plessis, A., 2017. Has snake fang evolution lost its bite? New insights from a structural mechanics viewpoint. *Biology Letters*, 13 (8), p.20170293. doi:10.1098/rsbl.2017.0293
- Broeckhoven, C., du Plessis, A., and Hui, C., 2017. Functional trade-off between strength and thermal capacity of dermal armor: insights from girdled lizards. *Journal of the Mechanical Behavior of Biomedical Materials*, 74, 189–194.
- Clymer, DR, Cagan, J, and Beuth, J, 2017. Power-velocity process design charts for powder Bed additive manufacturing. *Journal of Mechanical Design*, 139 (10), 100907–100907-7.



- Dong, G, Tang, Y, and Zhao, Y, **2017**. A survey of modeling of lattice structures fabricated by additive manufacturing. *Journal of Mechanical Design*, 139 (10), 100906–100906-13.
- Doube, M., et al., **2010**. BoneJ: free and extensible bone image analysis in ImageJ. *Bone*, 47 (6), 1076–1079.
- du Plessis, A., et al., **2017**. Prediction of mechanical performance of Ti6Al4 V cast alloy based on microCT-based load simulation. *Journal of Alloys and Compounds*, 724, 267–274.
- Fieres, J, Schumann, P, and Reinhart, C, **2018**. Predicting failure in additively manufactured parts using X-ray computed tomography and simulation. *Procedia Engineering*, 213, 69–78.
- Frazier, W.E, **2014**. Metal additive manufacturing: a review. *Journal of Materials Engineering and Performance*, 23 (6), 1917–1928.
- Freytag, M., Shapiro, V., and Tsukanov, I., **2011**. Finite element analysis in situ. *Finite Elements in Analysis and Design*, 47 (9), 957–972.
- Gibson, I., Rosen, D.W., and Stucker, B., **2010**. *Additive manufacturing technologies (Vol. 238)*. New York: Springer.
- Gibson, L.J., and Ashby, M.F., **1999**. *Cellular solids: structure and properties*. Cambridge: Cambridge university press.
- Gu, D.D., et al., **2012**. Laser additive manufacturing of metallic components: materials, processes and mechanisms. *International Materials Reviews*, 57 (3), 133–164.
- Hedayati, R., et al., **2016**. Mechanical properties of regular porous biomaterials made from truncated cube repeating unit cells: analytical solutions and computational models. *Materials Science and Engineering: C*, 60, 163–183.
- Hedayati, R., et al., **2018**. Comparison of elastic properties of open-cell metallic biomaterials with different unit cell types. *Journal of Biomedical Materials Research Part B: Applied Biomaterials*, 106 (1), 386–398.
- Hildebrand, T., et al., **1999**. Direct three-dimensional morphometric analysis of human cancellous bone: microstructural data from spine, femur, iliac crest, and calcaneus. *Journal of Bone and Mineral Research*, 14 (7), 1167–1174.
- Hildebrand, T., and Rüegsegger, P, **1997**. A new method for the model-independent assessment of thickness in three-dimensional images. *Journal of Microscopy*, 185 (1), 67–75.
- Hollister, S.J, **2005**. Porous scaffold design for tissue engineering. *Nature Materials*, 4 (7), 518–524.
- Lim, C.W.J., et al., **2016**. An overview of 3-D printing in manufacturing, aerospace, and automotive industries. *IEEE Potentials*, 35 (4), 18–22.
- Lopez-Heredia, M. A., et al., **2008**. Bone growth in rapid prototyped porous titanium implants. *Journal of Biomedical Materials Research Part A*, 85 (3), 664–673.
- Murr, L.E, **2017**. Open-cellular metal implant design and fabrication for biomechanical compatibility with bone using electron beam melting. *Journal of the Mechanical Behavior of Biomedical Materials*, 76, 164–177.
- Nouri A., Hodgson P.D., Wen C. **2009**. Biomimetic porous titanium scaffolds for orthopaedic and dental applications. In: M. Amitava ed., *Biomimetics, learning from nature*. Rijek, Croatia: Intech, 415–450.
- Orme, ME, et al., **2017**. Designing for additive manufacturing: lightweighting through topology optimization enables lunar spacecraft. *ASME. J. Mech. Des.*, 139 (10), 100905–100905-6.
- Parthasarathy, J., et al., **2010**. Mechanical evaluation of porous titanium (Ti6Al4 V) structures with electron beam melting (EBM). *Journal of the Mechanical Behavior of Biomedical Materials*, 3 (3), 249–259.
- Sallica-Leva, E., Jardini, A.L., and Fogagnolo, J.B, **2013**. Microstructure and mechanical behavior of porous Ti–6Al–4 V parts obtained by selective laser melting. *Journal of the Mechanical Behavior of Biomedical Materials*, 26, 98–108.
- Shapiro, V., and Tsukanov, I., **Jun. 1999**. Meshfree simulation of deforming domains. *Computer-Aided Design*, 31 (7), 459–471.
- Sing, S.L., et al., **2016**. Characterization of titanium lattice structures fabricated by selective laser melting using an adapted compressive test method. *Experimental Mechanics*, 56 (5), 735–748.
- Sing, S.L., Wiria F.E., and Yeong W.Y., **2018**. Selective laser melting of lattice structures: A statistical approach to manufacturability and mechanical behavior. *Robotics and Computer-Integrated Manufacturing*, 49, 170–180.
- Smith, M., Guan, Z., and Cantwell, W.J, **2013**. Finite element modelling of the compressive response of lattice structures manufactured using the selective laser melting technique. *International Journal of Mechanical Sciences*, 67, 28–41.
- Succi, S, **2001**. *The Lattice Boltzmann equation: for fluid dynamics and beyond*. Oxford: Oxford University Press.
- Tan, X.P., et al., **2017**. Metallic powder-bed based 3D printing of cellular scaffolds for orthopaedic implants: A state-of-the-art review on manufacturing, topological design, mechanical properties and biocompatibility. *Materials Science and Engineering: C*, 76, 1328–1343.
- Taniguchi, N., et al., **2016**. Effect of pore size on bone ingrowth into porous titanium implants fabricated by additive manufacturing: An in vivo experiment. *Materials Science and Engineering: C*, 59, 690–701.
- Thomsen, J.S., et al., **2005**. Stereological measures of trabecular bone structure: comparison of 3D micro computed tomography with 2D histological sections in human proximal tibial bone biopsies. *Journal of Microscopy*, 218 (2), 171–179.
- Vasconcellos, L. M. R., et al., **2010**. Evaluation of bone ingrowth into porous titanium implant: histomorphometric analysis in rabbits. *Brazilian Oral Research*, 24 (4), 399–405.
- Wang, X., et al., **2016**. Topological design and additive manufacturing of porous metals for bone scaffolds and orthopaedic implants: a review. *Biomaterials*, 83, 127–141.
- Yan, C., et al., **2015**. Ti–6Al–4 V triply periodic minimal surface structures for bone implants fabricated via selective laser melting. *Journal of the Mechanical Behavior of Biomedical Materials*, 51, 61–73.
- Zadpoor, A.A, **2017**. Mechanics of additively manufactured biomaterials. *Journal of the Mechanical Behavior of Biomedical Materials*, 70, 1–6.
- Zadpoor, A.A., and Hedayati, R, **2016**. Analytical relationships for prediction of the mechanical properties of additively manufactured porous biomaterials. *Journal of Biomedical Materials Research Part A*, 104A, 3164–3174.
- Zhang, X.Y., Fang, G., and Zhou, J, **2017**. Additively manufactured scaffolds for bone tissue engineering and the prediction of their mechanical behavior: a review. *Materials*, 10 (1), 50.